JOURNAL OF GEOPHYSICAL RESEARCH, VOL. 115, D03301, doi:10.1029/2009JD012023, 2010

Impact of the vertical velocity scheme on modeling transport in the tropical tropopause layer

F. Ploeger,[1] P. Konopka,[1] G. Günther,[1] J.-U. Grooß,[1] and R. Müller[1]

Received 6 March 2009; revised 25 August 2009; accepted 15 September 2009; published 2 February 2010.

[1] To assess the impact of the vertical velocity scheme on modeling transport in the tropical tropopause layer (TTL), 3 month backward trajectories are initialized in the TTL for boreal winter and summer 2002. The calculations are done in either a kinematic scenario with pressure tendency as the vertical velocity or in a diabatic scenario with cross-isentropic velocity deduced from various diabatic heating rates due to radiation (clear sky, all sky) and latent, diffusive and turbulent heating. This work provides a guideline for assessing the sensitivity of trajectory and chemical transport model (CTM) results on the choice of the vertical velocity scheme. We find that many transport characteristics, such as time scales, pathways and dispersion, crucially depend on the vertical velocity scheme. The strongest tropical upwelling results from the operational European Centre for Medium-Range Weather Forecasts kinematic scenario with the time scale for ascending from 340 to 400 K of 1 month. For the ERA-Interim kinematic and total diabatic scenarios, this time scale is about 2 months, and for the all-sky scenario it is as long as 2.5 months. In a diabatic scenario, the whole TTL exhibits mean upward motion, whereas in a kinematic scenario, regions of subsidence occur in the upper TTL. However, some transport characteristics robustly emerge from the different scenarios, such as an enhancement of residence times between 350 and 380 K and a strong impact of meridional in-mixing from the extratropics on the composition of the TTL. Moreover, an increase of meridionally transported air from the summer hemisphere into the TTL (maximum for boreal summer) is found as an invariant feature among all the scenarios.

Citation: Ploeger, F., P. Konopka, G. Günther, J.-U. Grooß, and R. Müller (2010), Impact of the vertical velocity scheme on modeling transport in the tropical tropopause layer, *J. Geophys. Res.*, *115*, D03301, doi:10.1029/2009JD012023.

1. Introduction

[2] Air in the tropics between an altitude of 14 and 20 km, equivalent to potential temperatures of 355 and 425 K, or pressures of 150 hPa and 70 hPa [*Fueglistaler et al.*, 2009a], shows a gradual transition from tropospheric to stratospheric characteristics [*Tuck et al.*, 1997; *Folkins et al.*, 1999; *Marcy et al.*, 2007]. The corresponding layer is termed the tropical tropopause layer (TTL) and is described in great detail by *Gettelman et al.* [2002] and *Fueglistaler et al.* [2009a]. In the following, we will frequently use the terminology of *Holton et al.* [1995] and call the tropical atmosphere above a potential temperature of about 380 K "stratospheric overworld" and the stratosphere poleward of the subtropical jets and below about 380 K "extratropical lowermost stratosphere."

[3] The TTL is considered to be rather important with respect to troposphere-to-stratosphere transport (TST) because it acts as a "gate to the stratosphere." Below the level of the "main convective outflow" around 350 K there is net upward transport due to convection. Above the level of zero radiative heating (LZRH), at about 360 K, the Brewer-Dobson circulation causes further ascent to the stratospheric overworld [*Holton et al.*, 1995], balanced by positive radiative heating [*Gettelman et al.*, 2004a]. However, the importance of different mechanisms, such as horizontal advection [*Holton and Gettelman*, 2001], convective overshooting [*Danielsen*, 1982], in particular above continental areas [*Ricaud et al.*, 2007] and mixing [*Konopka et al.*, 2007], for transport from the main convective outflow to the stratosphere is still an open issue. Moreover, there is the associated question of the extent to which the upwelling air in the TTL is isolated from or exchanged with the extratropical lowermost stratosphere (transport from the extratropics into the TTL will be termed "in-mixing" in the following). Concentrations of trace gas species with tropospheric sources (e.g., very short-lived substances (VSLS), water vapor) in the overworld and lowermost stratosphere greatly depend on whether upwelling tropospheric air is mainly directed upward or meridionally transported out of the tropics. Therefore, transport across the TTL impacts stratospheric water vapor trends and stratospheric chemistry. It is also subject to climate change.

[4] Several model studies of transport across the TTL have recently been presented, based on both trajectory calculations and CTMs [*Fueglistaler et al.*, 2004, 2005; *Bonazzola and Haynes*, 2004; *Konopka et al.*, 2007; *Levine*

[1]Institute for Stratospheric Chemistry, Forschungszentrum Jülich, Jülich, Germany.

0148-0227/10/2009JD012023$09.00

et al., 2007, 2008; *Kremser et al.*, 2009] which were driven by either assimilated reanalysis or global climate model meteorological data.

[5] Usually two types of vertical transport schemes are employed, referred to as ''diabatic'' and ''kinematic'' [*Schoeberl et al.*, 2003]. Diabatic denotes transport calculations in an isentropic coordinate system with cross-isentropic motion determined from diabatic heating rates, while kinematic stands for horizontal transport along pressure surfaces with the pressure tendency as the vertical velocity. The nearly adiabatic nature of the large-scale motion in large parts of the atmosphere, with the flow mainly being along surfaces of constant potential temperature, seems to favor an isentropic coordinate system. Recent studies indicate that in a diabatic scenario the unrealistically high vertical dispersion due to the pressure tendency velocity can be reduced [*Schoeberl et al.*, 2003] and the cold-point sampling becomes more focused on regions of lower than tropical mean temperatures [*Krüger et al.*, 2008, 2009]. There are approaches to carry the advantages of diabatic scenarios over to kinematic scenarios [*Wohltmann and Rex*, 2008].

[6] Most studies on transport across the TTL were performed in a kinematic scenario [*Fueglistaler et al.*, 2004; *Bonazzola and Haynes*, 2004; *Levine et al.*, 2007]. For diabatic scenarios the radiative heating rates are frequently calculated offline, using radiative transfer calculations [*Krüger et al.*, 2008]. Contributions due to latent heat release are significant only below approximately 360 K, where water vapor mixing ratios are large. Thus, in studies focusing on regions above 360 K, heating rates due to latent heat release are sometimes neglected [e.g., *James et al.*, 2008]. In order to model transport through the whole range from the troposphere to the stratosphere, however, they must be included in the energy budget to derive vertical velocities from total diabatic heating rates.

[7] ERA-Interim reanalysis and forecasts [*Simmons et al.*, 2006; *Uppala et al.*, 2008] from the European Centre for Medium-Range Weather Forecasts (ECMWF) are a comparatively new meteorological data set for modeling atmospheric transport and will be used in this work, together with operational ECMWF analysis data. To study only advective transport, we choose a pure trajectory approach. The model in use is the trajectory module of the Chemical Lagrangian Model of the Stratosphere, CLaMS [*McKenna et al.*, 2002; *Konopka et al.*, 2007]. It can be run in the diabatic and the kinematic mode.

[8] In this work, we will compare different types of vertical velocities and their consequences for modeling atmospheric processes. Our main objective, i.e., the impact of the vertical velocity scheme on transport in the TTL, will be broken down into the following questions: (1) How large are the differences with respect to pathways and time scales of transport across the TTL between diabatic and kinematic scenarios? (2) How do the various contributions in the diabatic heat budget affect the characteristics of transport to the stratosphere? In particular, we will investigate how a stronger or weaker tropical circulation favors different compositions of the TTL (vertically upwelling versus meridionally in-mixed air) and pathways of TST.

[9] Transport characteristics such as time scales and pathways will be classified as either ''sensitive'' or ''robust'' in the discussion. This notation elucidates which modeled characteristics are largely sensitive, depending on the chosen scenario, and which emerge as a robust picture from all scenarios.

[10] In section 2 we briefly describe the model setup with seven scenarios of different vertical velocities. In section 3 we analyze transport into the TTL and in section 4 transport across the TTL. We conclude with a discussion of the results in section 5.

2. Data and Method

[11] The vertical velocity $\mathrm{d}\theta/\mathrm{d}t$ in isentropic coordinates (potential temperature θ as vertical coordinate) is deduced from the diabatic heating rate Q via the thermodynamic equation [*Andrews et al.*, 1987]

$$c_p \frac{\mathrm{d}\theta}{\mathrm{d}t} = Q\frac{\theta}{T}, \tag{1}$$

with T denoting temperature and c_p the specific heat capacity at constant pressure. As heating rates are not stored in standard ECMWF operational analysis data, we use the new ERA-Interim data set of meteorological reanalysis and forecasts [*Simmons et al.*, 2006; *Uppala et al.*, 2008], which provides this information. Its usage allows transport to be modeled in isentropic coordinates in the stratosphere and upper troposphere, including the entire TTL, with the vertical velocity given by equation (1).

2.1. ERA-Interim Data

[12] The basis for our investigations is the ERA-Interim data set from the ECMWF and also operational ECMWF data, for comparison. Heating rates from ERA-Interim were shown to have a much better quality than those from ERA-40 [*Fueglistaler et al.*, 2009b], which exhibit a rather excessive tropical circulation [*Uppala et al.*, 2005; *Monge-Sanz et al.*, 2007] and unrealistic oscillations in the high-latitude heating field [*Fueglistaler et al.*, 2009b].

[13] The heating rate information is taken from ERA-Interim forecast data. To be more precise, the 6 h forecasts at 0000/1200 UTC provide heating rates for the 0600/1800 UTC reanalyses, while the 12 h forecasts the heating rates for the 1200/0000 UTC reanalyses. The forecasts include heating rates due to clear-sky radiation (Q_{csk}), clear-sky radiation with effects of clouds (all-sky radiation, Q_{ask}) and the total diabatic heating rate (Q_{tot}). We furthermore compute the heating rate due to latent heat release, diffusive and turbulent heat transport as a residual heating rate by subtracting the all-sky from the total heating term, $Q_{\tilde{\mathrm{res}}} = Q_{\mathrm{tot}} - Q_{\mathrm{ask}}$. *Fueglistaler et al.* [2009b] already mentioned that it is not possible to separate the latent heating rate alone, but only the term $Q_{\tilde{\mathrm{res}}}$, comprising the sum of latent heat exchange and diffusive and turbulent heat transport. For our further calculations, we redefine the residual heating rate as $Q_{\mathrm{res}} = Q_{\tilde{\mathrm{res}}} + Q_{\mathrm{csk}}$. Because above about 360 K, the region of main interest for this work, clear-sky radiative heating makes the largest contribution to the diabatic heating (see, e.g. Figure 1, explained in detail below), we may think of clear-sky radiation as a heating ''background,'' to which the effects of radiation with clouds and of residual heating are added.

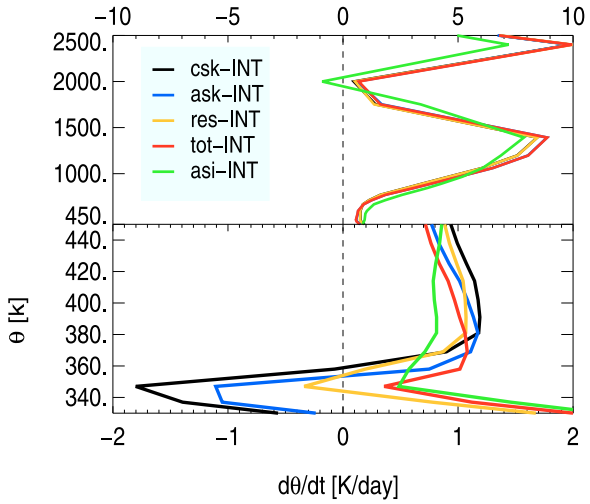

Figure 1. Annual mean tropical vertical velocity dθ/dt (±10° latitude, 2002) for the different diabatic tendencies, inferred from ERA-Interim. Note the different scalings of the abscissa in the top and bottom parts of the plot.

[14] Further, a heating rate due to the assimilation procedure (the assimilation increment) is derived, as described by *Fueglistaler et al.* [2009b] and added to the total diabatic heating rate for our calculations. In the following, assimilation increment denotes the total $Q_{\mathrm{asi}} = c_p(T_{\mathrm{an}} - T_{\mathrm{fc}})/\Delta t_{\mathrm{fc}} + Q_{\mathrm{tot}}$. Here, T_{an} denotes reanalysis, T_{fc} forecast temperature and Δt_{fc} the forecast time step. The assimilation increment is required to close the heating budget and is interesting to look at, as it represents that part of the heating resulting from disagreements between model and observations.

[15] To summarize, this work is based on five isentropic scenarios from ERA-Interim with different diabatic heating rates. In the following, these are denoted csk-INT (clear sky, Q_{csk}), ask-INT (all sky, Q_{ask}), res-INT (residual, Q_{res}), tot-INT (total, Q_{tot}) and asi-INT (assimilation, Q_{asi}). Moreover, we will also consider the two isobaric scenarios of ERA-Interim and operational ECMWF data on pressure levels together with the corresponding pressure tendency ω, denoted ω-INT and ω-OP. Table 1 summarizes the seven scenarios of different vertical velocities, which will allow us to quantify the effects of various physical parameters (clear-sky heating rates, cloud and residual heat effects) on transport as well as to compare the diabatic to the kinematic approach and the interim to the operational ECMWF data.

[16] To simplify the interpretation of our results in the following, we first consider the tropical upwelling in the five isentropic scenarios. Figure 1 shows profiles of the corresponding zonal mean tropical vertical velocities dθ/dt, annually averaged between ±10° latitude. Figure 1 is divided into a bottom plot (potential temperature range of 330–450 K) and a top plot (450–2500 K) with different scalings of the abscissa to account for the range of magnitude of the vertical velocities.

[17] The most striking feature of the clear-sky velocity (Figure 1, black line) is its sharp decrease from 1.2 K/d to −1.8 K/d, crossing the zero baseline around 360 K, the LZRH. The effects of clouds and residual heating (blue and gold lines) in the ERA-Interim data set displace this level to lower potential temperatures and reduce the negative values below and the positive values above, respectively, consistent with the results of *Fueglistaler and Fu* [2006]. The combined effects of clouds and residual heating (total diabatic heating (Figure 1, red line)) finally yield a continuously positive vertical velocity.

[18] A slight minimum remains around a potential temperature level at about 350 K, between the top of the tropospheric Hadley and the lower end of the stratospheric Brewer-Dobson circulation. It remains to be shown whether this minimum is of physical origin or just an artefact of the ECMWF model. Furthermore, the assimilation increment weakens the sharpness of the minimum as it attenuates the upwelling above and amplifies the upwelling below.

2.2. Trajectory Setup

[19] Backward trajectories are initialized on a 1° × 1° horizontal grid between latitudes of ±30°N and 0° and 360° longitude on nine θ levels in the vertical between 340 K and 420 K, with a vertical spacing of 10 K. Altogether, this yields a total of about 200,000 trajectories, which are started twice, on 1 March 2002 and on 30 August 2002, and calculated backward for 90 days. Thus boreal winter (djf) and summer (jja) are both covered. We verified the insensitivity of the results against slight variations of initialization dates (1 day/month earlier).

[20] We use backward trajectories to explore the origin of air reaching the TTL and the lower stratospheric overworld and the respective pathways from the troposphere. Of course, the interpretation of results of single trajectories over a period of 3 months would be misleading. However, inferring statistical properties of real atmospheric transport from a large ensemble of trajectories is a reliable method.

[21] For the trajectory calculations we use the trajectory program CLaMS-TRAJ which is part of the Lagrangian chemical transport model CLaMS [*McKenna et al.*, 2002; *Konopka et al.*, 2007]. It can be run using either pressure or potential temperature as the vertical coordinate with

Table 1. Definitions of the Different Vertical Velocity Scenarios

Scenario	Data Set	Vertical Coordinates	Vertical Velocity	Line Style[a]
csk-INT	ERA-Interim	θ	$\sim Q_{\mathrm{csk}}$: clear-sky radiation	black (solid)
ask-INT	ERA-Interim	θ	$\sim Q_{\mathrm{ask}}$: all-sky radiation	blue (solid)
res-INT	ERA-Interim	θ	$\sim Q_{\mathrm{res}}$: residual heating = latent + mixing + clear-sky	gold (solid)
tot-INT	ERA-Interim	θ	$\sim Q_{\mathrm{tot}}$: total heating	red (solid)
asi-INT	ERA-Interim	θ	$\sim Q_{\mathrm{asi}}$: assimilation increments + total heating	green (solid)
ω-INT	ERA-Interim	p	$\omega = \mathrm{d}p/\mathrm{d}t$	gray (solid)
ω-OP	operational ECMWF	p	$\omega = \mathrm{d}p/\mathrm{d}t$	black (dash-dotted)

[a]Line styles used in all figures.

pressure tendency or diabatic heating rate, respectively, as the vertical velocity. For the computations in the kinematic scenarios the meteorological data was interpolated from the ECMWF hybrid vertical coordinate to 28 pressure levels with vertical velocity $\omega = dp/dt$. For the diabatic calculations the meteorological data was interpolated to 45 potential temperature levels and the vertical velocity $d\theta/dt$ calculated as one of the five different diabatic heating rates, as described in section 2.1. The levels covering the TTL for the kinematic and diabatic scenarios are 200, 140, 100, 90, 70, 50 hPa and 358, 369, 381, 391, 402, 414, 425 K, respectively.

[22] For our analysis, we view the TTL as being laterally confined by ±30° equivalent latitude (approximately the tropical edge of the subtropical jet core) and consider only the subset of trajectories starting in this equivalent latitude range (except for Figure 6) throughout this work. We verified the insensitivity of all results with respect to slight variations of equivalent latitude bounds and with respect to replacing equivalent latitude by latitude bounds.

[23] It should be noted that in our work the term in-mixing refers to trajectories entering the tropics from outside the ±30° equivalent latitude band, irrespective of potential former crossings of these boundaries. The connection to in-mixing of air masses from the extratropical lowermost stratosphere into the TTL will be discussed in section 5.2.3.

3. Transport Into the TTL

[24] There are two possibilities of entering the TTL, either across its vertical (from below: tropical troposphere; from above: stratospheric overworld) or across its meridional boundaries (extratropical lowermost stratosphere). To investigate these "gates to the TTL" in our various scenarios of vertical velocities we consider the TTL at the initialization time as being composed of those trajectories, which are started in the range $360 \leq \theta \leq 400$ K and between ±30°N equivalent latitude. In the following, we calculate the fractions of these TTL trajectories crossing a certain meridional or vertical boundary during the time of backward integration and refer to them as "fractions of air" entering the TTL. To reduce the influence of transient transport across the boundaries and the influence of interpolation we determine the locations where the TTL trajectories (or "air parcels") cross either the vertical boundaries 350 K/410 K, or the meridional boundaries ±35°N (equivalent latitude) of a larger region.

[25] Figure 2 shows the probability density functions (PDFs) of the locations where the TTL trajectories crossed the boundaries of the larger region defined above. All distributions in this section are normalized to the total amount of trajectories initialized in the TTL. The plot in the middle of each panel in Figure 2a displays the two-dimensional PDF for crossing the lower boundary of 350 K (the number of crossing events is binned in approximately 2° latitude/6° longitude bins). The upper and lower plots of each panel show the one-dimensional PDFs for crossing the meridional boundaries, with a bin size of 10° longitude. Thus Figure 2a allows vertical transport to be compared with horizontal transport into the TTL.

[26] The effects on the locations of entry from below are less distinct (Figure 2a, gray PDFs, underlaid with continents, in the middle of each panel). Nevertheless, there are differences. Thus for the diabatic scenarios, in particular during boreal summer, the main entry region is located more to the north than for the kinematic scenarios. In the latter cases, the peak of the distribution is more zonally symmetric. The specific pattern with the main entry region above the Western Pacific for boreal winter and displaced northwestward (above South China Sea/Indian Ocean/India) for boreal summer is left unaltered for all scenarios.

[27] The shape of the distributions of the meridional entry locations is similar for the various scenarios (Figure 2a, top/bottom of each plot). In all scenarios (only tot-INT and ω-OP shown), the strongest meridional in-mixing occurs in the summer hemisphere above the Western/Central Pacific and the Indian Ocean/India regions. For boreal summer, there is an increasing number of trajectories entering the TTL from the northern hemisphere (NH; southern hemisphere will be denoted SH) extratropics, which is even higher for the diabatic than for the kinematic scenario. All summer distributions peak roughly at longitudes of the equatorial Western Pacific/Northern India/Caribbean.

[28] Figure 2b further elucidates the meridional in-mixing, showing the PDFs of potential temperatures of crossing the meridional boundaries. Irrespective of the scenario, the main region of meridional in-mixing is located around 380 K. Below 380 K the subtropical jets act as a transport barrier (strongest in the winter hemisphere, in particular during boreal summer) inhibiting exchange between tropics and extratropics [*Haynes and Shuckburgh*, 2000]. Only for boreal summer is the transport barrier less efficient and a large fraction of trajectories enters the TTL directly above the LZRH. The peak of the distribution is highest for the clear-sky scenario with trajectories entering the TTL exclusively above the LZRH, at approximately 360 K. In the other diabatic and in the kinematic scenarios, the meridional in-mixing can happen below the LZRH as well.

[29] Figure 3 shows how far the trajectories reach into the extratropics. The almost linear decrease of the fraction of TTL trajectories reaching regions poleward of a particular equivalent latitude shows that a certain number of in-mixed trajectories are only transported through subtropical regions (not reaching equivalent latitudes poleward of ±50°). But, in particular for boreal summer in the NH, a certain number of in-mixed trajectories are also transported through high-latitude regions.

[30] To simplify the comparison of the various scenarios we consider the total fractions of trajectories entering the TTL across a certain boundary for boreal winter and summer 2002 in the schematic of Figure 4. It is evident that for clear-sky diabatic heating (csk-INT) no air enters from below the LZRH, but all the air comes from the extratropics. In this case, the negative vertical velocities below the LZRH constitute an impermeable vertical transport barrier. The fraction of trajectories entering the TTL from below increases for the all-sky and residual heating scenario (about 70/35% for djf/jja, not shown) and even further for the tot-INT, asi-INT and the kinematic scenarios (about 75/60%). The sum of the four meridional and vertical fractions for each scenario in Figure 4 does not always yield 100% because a certain number of trajectories do not leave the TTL during the 3 months of backward integration.

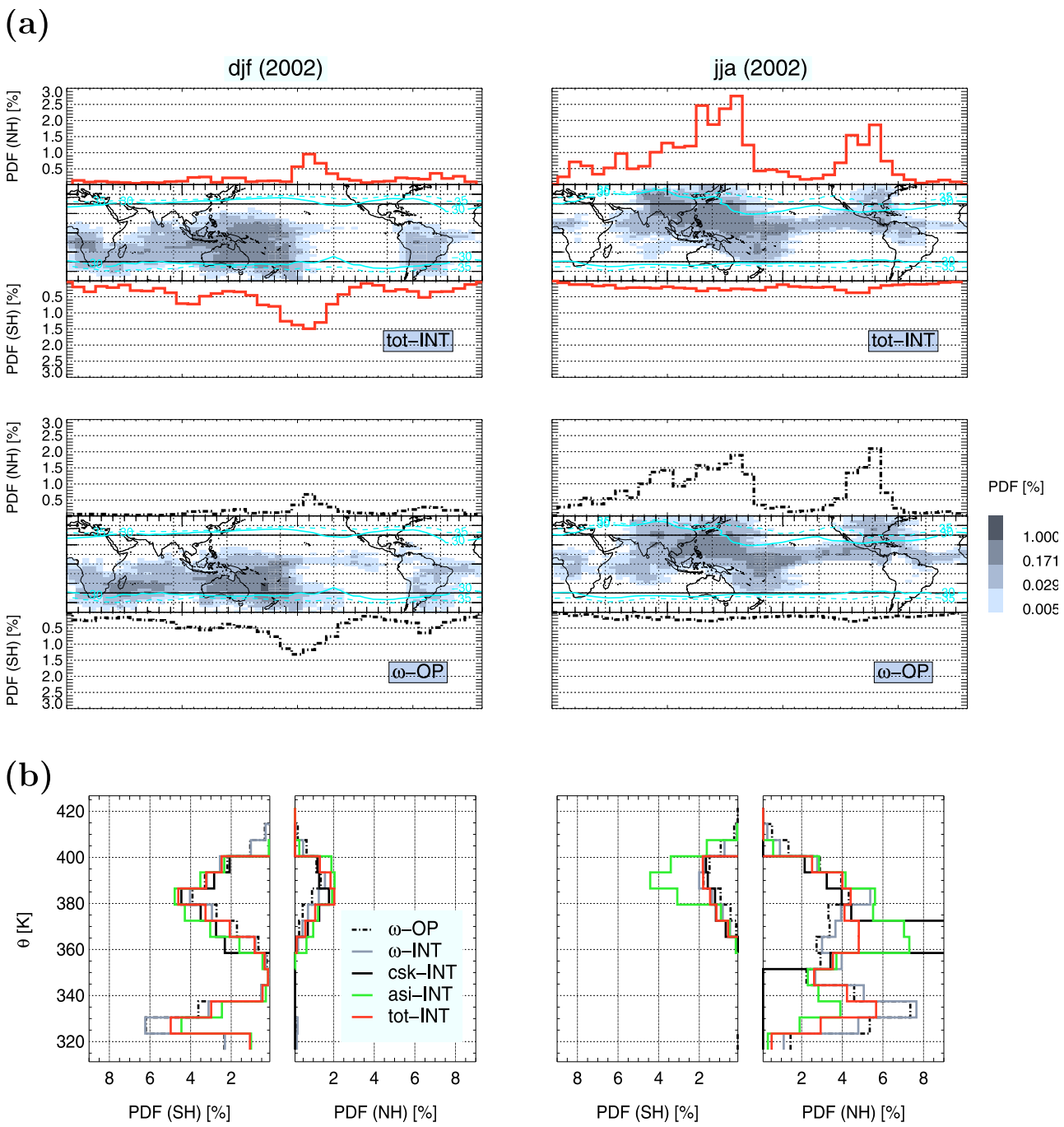

Figure 2. Vertical versus horizontal transport into the TTL for (left) December-January-February (djf) and (right) June-July-August (jja). (a) The gray color scheme shows regions of vertical transport into the TTL (PDF of entry locations at 350 K) for (top) tot-INT and (bottom) ω-OP; notice the nonlinear color scale. The thin solid black/solid cyan and dashed cyan lines show the ±30° latitude/±30° and ±35° equivalent latitude contours, as averages in the 350–400 K layer for the respective djf/jja period. The solid/dashed lines in the bottom and top areas of each plot describe PDFs of locations where the TTL trajectories crossed the meridional boundaries (±35°N equivalent latitude), as functions of longitude. (b) PDFs of potential temperatures where the northern and southern hemispheric meridional boundaries are crossed (the peak value for csk-INT/jja is 27.5%). All distributions are normalized to the total number of trajectories initialized in the TTL.

[31] We will now compare in more detail the four scenarios tot-INT, asi-INT, ω-INT and ω-OP, which involve the complete heating budget and therefore are assumed to represent the real atmosphere best. Using operational ω as the vertical velocity 21/32% of the air in the TTL enters from the extratropics for boreal winter/summer, while for interim ω these fractions increase to 23/36%, for total diabatic heating to 24/36% and for the assimilation incre-

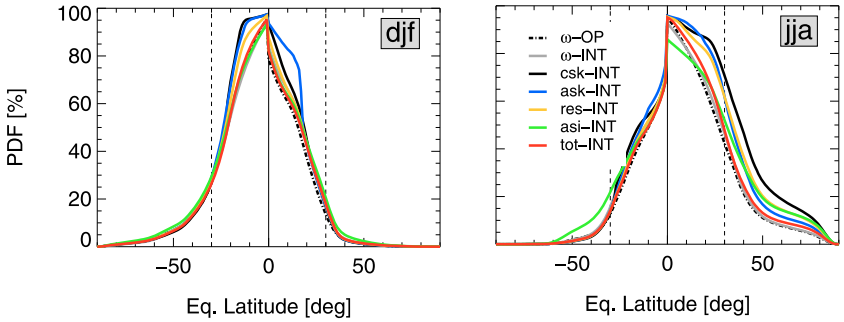

Figure 3. Fractions of TTL trajectories which reach regions poleward of a particular equivalent latitude (above 340 K) during 3 months: (left) djf and (right) jja.

ment scenario even to 29/52%. For these four scenarios almost all the air in the TTL originates from outside its boundaries during 3 months, evident from the total of the fractions in Figure 4, which almost always yields 100%.

[32] Despite all the differences between the scenarios with respect to exact numbers there are several properties common to all. First, for the four realistic scenarios (tot-INT, asi-INT, ω-INT and ω-OP), there is a rather similar pattern of entry into the TTL across the vertical and meridional boundaries (Figure 4). The in-mixed fraction from the extratropics is always larger for boreal summer (33–50%) than for boreal winter (approximately 25%). Second, in the summer hemisphere there is always a much larger fraction of air entering the TTL across the meridional boundary than in the respective winter hemisphere. The maximum difference between the two hemispheres arises during boreal summer, in particular between 360 K and 380 K. Figure 4 shows more precisely that irrespective of the vertical velocity used there is at least twice as much meridional in-mixing from the summer than from the winter hemisphere. However, the absolute fractions vary, depending on the scenario.

4. Transport Across the TTL

[33] Following *Fueglistaler et al.* [2004], we examine the characteristics of transport in the TTL for our seven scenarios of different vertical velocities. In particular, we will show how the different diabatic heating contributions cause transport from the level of the main convective outflow to the stratosphere and determine the characteristics of the TTL as a transitional zone.

4.1. Trajectory Fractions

[34] The notation of Figure 5 is the same as that of *Fueglistaler et al.* [2004]. Thus with $f^{\leftarrow,\theta_0}(\theta)$ we denote the fraction of backward trajectories starting at θ_0, which reach θ during the considered period. Figure 5a displays the fraction of trajectories initialized at 400 K, which ascended from below θ during the first 60 days after release. In a hypothetical atmosphere with an impermeable transport barrier between troposphere and stratosphere, this curve should approximate to 1 above and 0 below the barrier. Obviously, the curve for clear-sky radiative heating (solid black) comes very close to this idealized case, with the boundary exactly at the level of zero clear-sky radiative heating. Therefore, a large fraction of the air at 400 K ascended from around 360 K, but none from below, depicting the fact of negative vertical velocities below ~360 K (Figure 1). Figure 5a further indicates a slightly higher potential temperature of the LZRH for boreal summer compared to boreal winter.

[35] The effects of clouds lower this level by 5–10 K. Residual heating (latent and mixing heating) yields enough upwelling to cause transport from the troposphere to the stratosphere, at least for boreal winter. The combined effects of clouds and residual heating finally yield a transition zone, in which the amount of air reaching 400 K from below a certain potential temperature level gradually increases as this level approaches 400 K.

[36] For boreal winter as well as for summer, the tropical upwelling due to ω from operational ECMWF meteorological analysis is the strongest, with about 60/50% (for djf/jja) of the air at 400 K originating below 340 K during a period of 60 days (Figure 5a). For total diabatic heating (red curve) this fraction is reduced to ~40/20% for boreal winter/

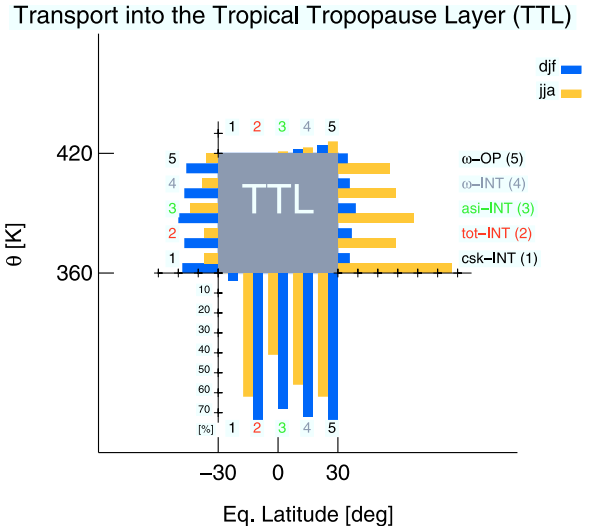

Figure 4. Fractions of trajectories entering the TTL across a particular vertical (top: from above; bottom: from below) or meridional (right: from NH; left: from SH) boundary for boreal winter (blue) and summer (gold) 2002.

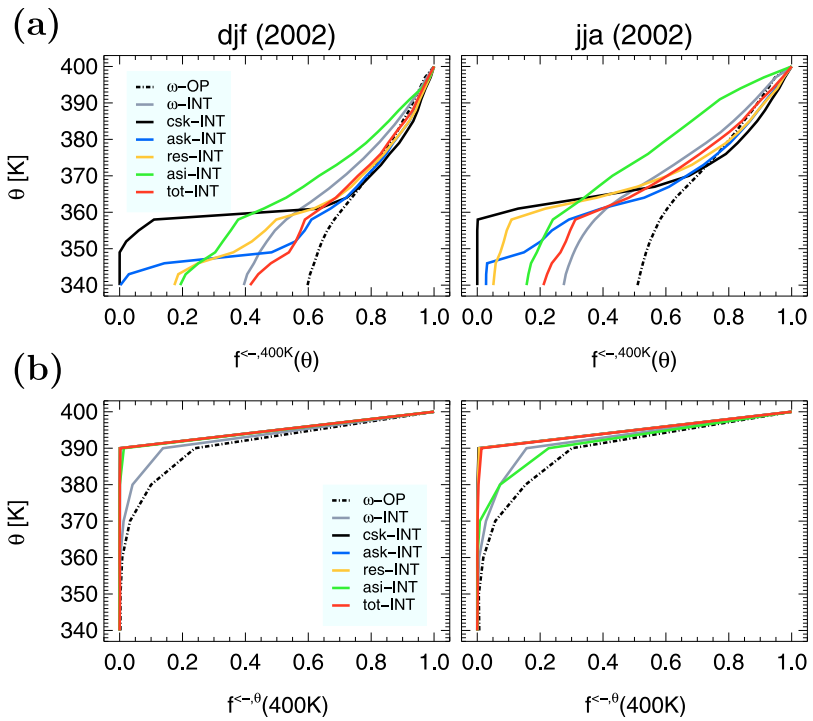

Figure 5. (a) Fractions of backward trajectories starting at 400 K, which ascended from below θ during the first 60 days after release. (b) Fractions of backward trajectories starting at θ, which descended from above 400 K, during the same period as in Figure 5a. Note that the other diabatic lines in Figure 5b are covered by the tot-INT line.

summer. The curve for ω from ERA-Interim (solid gray) stays close to the diabatic scenario from the same data set. An interesting fact is the large discrepancy between tot-INT and asi-INT for boreal summer, indicating a strong impact of the assimilation increment.

[37] Figure 5b further elucidates the impact of the assimilation increment. It displays the fraction of trajectories at a certain level, which descended from above 400 K during the previous 60 days. For boreal winter, the picture seems rather clear. In the diabatic scenarios no air in the TTL below 400 K stems from above 400 K, even at the next lower level of 390 K. By contrast, in the kinematic scenarios nonvanishing fractions of air (~25% at 390 K for ω-OP) originate at potential temperatures higher than 400 K. This property of subsidence was already mentioned by *Fueglistaler et al.* [2004] and is also evident in the assimilation increment scenario asi-INT for boreal summer. It will be discussed further in section 5.1.1.

[38] The reason for these quite different characteristics of air motion is hidden in the structure of the vertical velocity fields. To elucidate this fact, we calculate the average cross-isentropic velocity $d\theta/dt$ along all the trajectory positions for the boreal winter trajectory ensemble between 380 K and 400 K. These "net heating fields" are binned on a horizontal grid (1° × 1° latitude/longitude) and averaged over the three winter months. Figure 6 depicts the "net heating fields" and shows that they are very different for the diabatic scenarios csk-INT, tot-INT and the kinematic scenario ω-INT (results in Figure 6 are derived from all trajectories, without any equivalent latitude restriction). In a "diabatic world" there is almost no subsidence in the upper TTL (average $d\theta/dt$ everywhere positive), while in a "kinematic world" subsidence frequently occurs. The assimilation increment consequentially yields a scenario in between, with regions of subsidence less distinct than in the kinematic scenarios.

[39] The picture for boreal summer changes only slightly (not shown). However, for asi-INT the regions of subsidence increase for boreal summer (not shown), as expected from the fractions of descending trajectories at 390 K in Figure 5b.

[40] The property of subsidence in the TTL in the isobaric ω scenarios also appears in the vertical dispersion of trajectories starting at 400 K in the (equivalent latitude/θ) plane, displayed in Figure 7 (similar to Figure 2 of *Sparling et al.* [1997]). For the total diabatic scenario the distribution of parcel locations is quite distinct, with the majority ascending from below through the lower and mid TTL. On the contrary, ω as the vertical velocity leads to much higher vertical dispersion. The assimilation increment scenario is again located in between.

[41] The "Ψ shape" of the distribution in the ω-INT and ω-OP plots of Figure 7 for the two kinematic scenarios confirms the subsidence in Figure 5b, with the trajectories located directly above their initialization level in Figure 7 subsiding to 400 K during the backward integration period.

4.2. Time Scales of Transport in the TTL

[42] In Figure 8 we consider residence times Δt_{res} for trajectories in a layer around a particular potential temperature θ. These residence times are computed by averaging

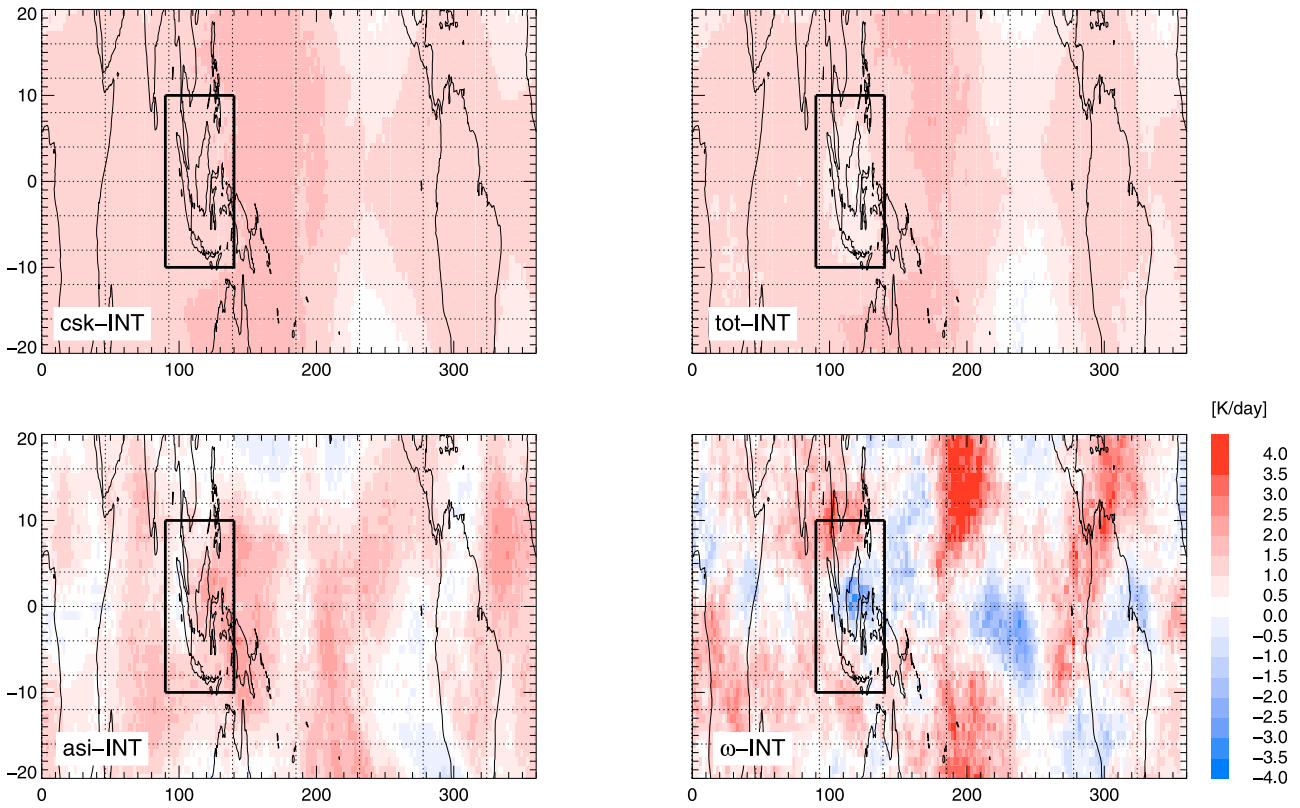

Figure 6. Mean cross-isentropic velocity $d\theta/dt$ in the upper TTL (380 K $\leq \theta \leq$ 400 K) calculated from the cross-isentropic motion of the trajectory ensemble for NH winter (djf). The black rectangular depicts the maritime continent.

the durations for leaving the layer [$\theta-10$ K, $\theta + 10$ K] over the ensemble of trajectories initialized at θ, as was done by *Fueglistaler et al.* [2004]. Figure 8 shows that operational ω (ω-OP) yields residence times very similar to the residence times of *Fueglistaler et al.* [2004], as it stems from the same data set, only for a different year.

[43] A comparison of the ask-INT and csk-INT scenarios shows that the radiative effects of clouds accelerate the upwelling below 380 K (heating in cloud layer) and retard it above (cooling above cloud layer), in agreement with *Fueglistaler and Fu* [2006]. Nevertheless, for clear-sky radiative heating rates with either the addition of cloud effects or latent and mixing heating the ascent below 380 K remains very slow. However, the combined effect of clouds, latent and mixing heating yields residence times which are comparable to the kinematic case ω-INT. Overall, the residence times per 10 K for the interim total diabatic scenario are 2–5 days longer than for the kinematic ω-INT scenario. The operational kinematic data exhibits the strongest tropical upwelling with residence times per 10 K as much as 2–7 days shorter than for ω-INT. Further, we want to stress again the larger effects of the assimilation increment during boreal summer compared to winter, attenuating the upwelling mainly above about 360 K.

[44] A different way to quantify transport time scales is to consider the full age distribution of trajectories. In the theory of age spectra [*Hall and Plumb*, 1994; *Waugh and Hall*, 2002; *Schoeberl et al.*, 2003], the term age corresponds to the transit time of an air parcel between two locations and age spectrum to the distribution of these ages within a given volume of air.

[45] Below we discuss the transit time distribution for parcels initialized at 400 K for transport from 340 to 400 K. The respective transit time distributions for boreal winter in Figure 9 (left) reveal that operational ω yields a much larger number of rapidly ascending trajectories than ω from ERA-Interim. Moreover, the ascent due to total diabatic heating turns out to be much slower, with the fastest trajectories lagging behind the fastest ones of the kinematic scenarios by ~20 days.

[46] The mean time scales for ascent from the troposphere to the stratospheric overworld are given in Table 2 as the mean ages. As we noted already, ω from operational data yields the fastest transport to the overworld with a mean age $\overline{\Delta t_{400\leftarrow 340}}$ = 33/33 days for djf/jja, while the time scales for ω-INT and for tot-INT are up to a month longer. For boreal summer (jja) in the interim scenarios there are much less rapidly transported trajectories than for (djf), whereas the distribution for operational data changes only slightly.

[47] Further, the effect of adding the assimilation increment to the diabatic heating appears to be contrary in the two seasons. During boreal winter the use of assimilation increments as heating rates reduces the amount of fast trajectories, while during summer it accelerates the fastest ones even more (Figure 9, right).

[48] There is still another difference between the age spectra for the kinematic and diabatic scenarios. While for ω-OP the distribution for djf has one broad peak at short times

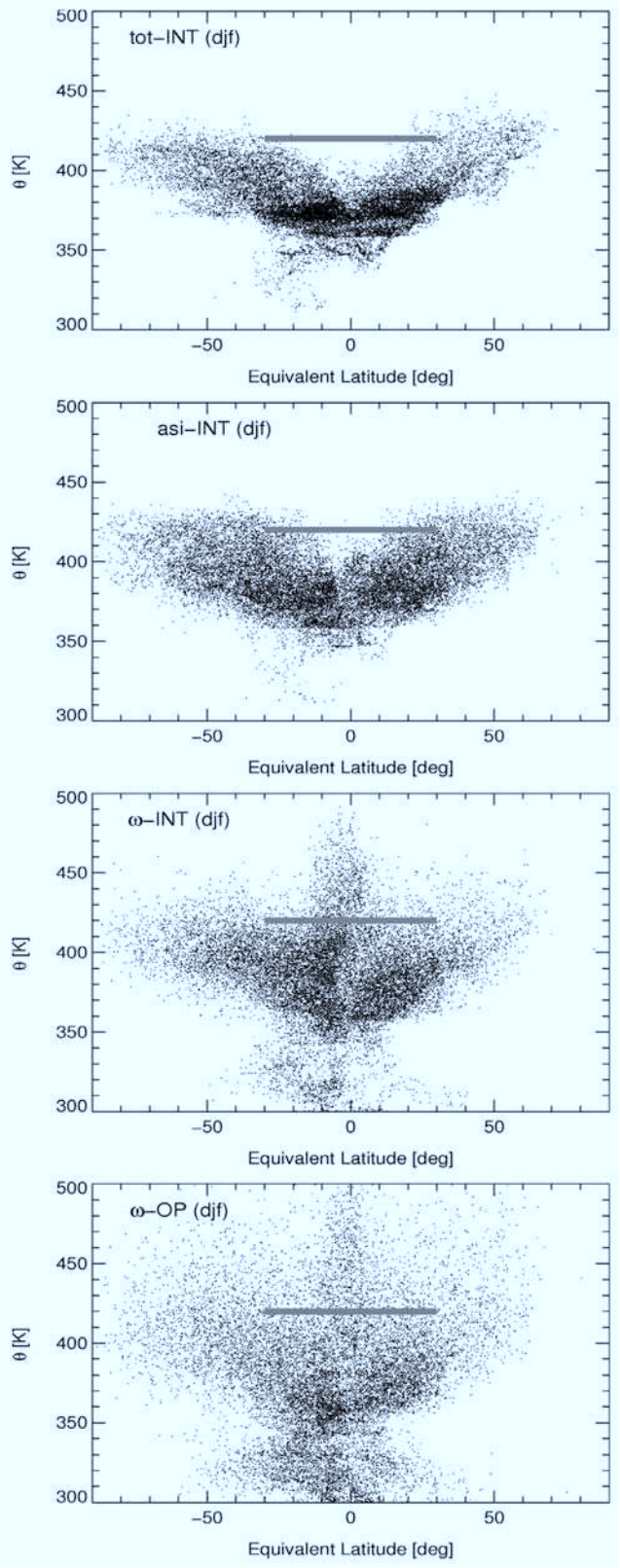

Figure 7. Vertical dispersion of trajectories, starting at 400 K, in the (equivalent latitude/θ) plane after 45 days of backward integration for NH winter (djf). The gray bar displays the initialization locations (top to bottom: scenarios tot-INT, asi-INT, ω-INT, and ω-OP).

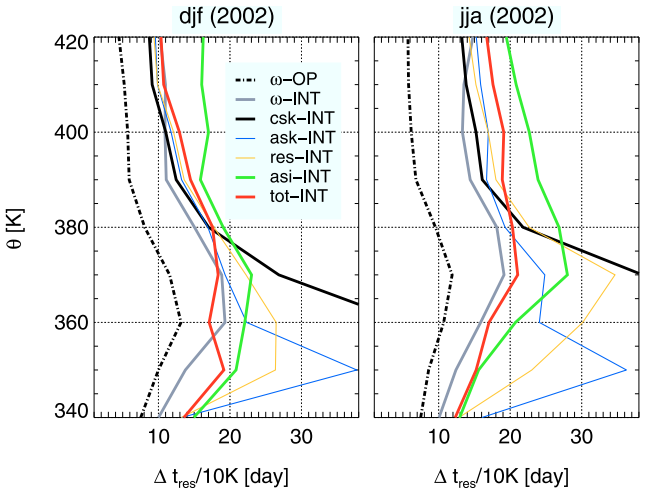

Figure 8. Mean residence time Δt_{res} of trajectories for staying in a 10 K layer around θ.

(25 days), the diabatic heating rate scenario surprisingly shows a two-peak shape (first peak at ~35, second peak at ~60 days) indicating two separate transport pathways. The second peak can also be seen in the ω-INT scenario, albeit less distinctly, and will be discussed in section 5.1.4.

5. Discussion

[49] To summarize how sensitively transport characteristics depend on the vertical velocity scheme we classify them as either sensitive or robust in Table 3. Results with respect to sensitive characteristics are largely sensitive, strongly depending on the choice of vertical velocity. On the other hand, results concerning robust characteristics emerge as a robust picture, irrespective of the vertical velocity used. In the following, we will discuss these sensitive (subsidence, dispersion, residence times, pathways) and robust (residence time enhancement, gates to the TTL, in-mixing, hemispheric asymmetry of in-mixing) characteristics.

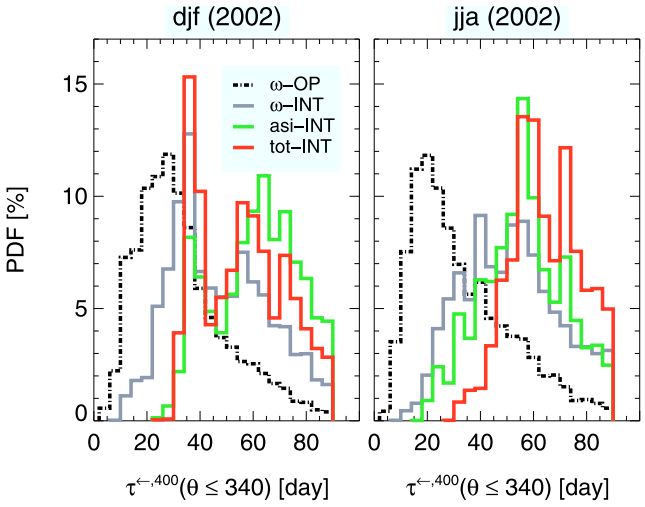

Figure 9. Transit time distributions at 400 K for the upward transport from 340 K. The bin size is 4 days.

Table 2. Mean Transit Times for Ascent Across the TTL[a]

	csk-INT	ask-INT	res-INT	tot-INT	asi-INT	ω-INT	ω-OP
$\overline{\Delta t}_{400\leftarrow340}$		77/71	64/68	56/64	61/56	47/51	33/33
$\overline{\Delta t}_{400\leftarrow370}$	32/42	33/42	35/46	36/46	39/37	26/33	16/17

[a]Times given in days (the notation is djf/jja).

5.1. Sensitive Transport Characteristics

5.1.1. Subsidence in the TTL

[50] It was suggested by *Sherwood* [2000] that air which detrains from overshooting convective turrets subsides in the region above deep convective systems. The rise into the stratosphere consequently occurs at different locations. The most important region of subsidence, the 'stratospheric drain' region, was found above the maritime continent, with positive pressure tendencies along the 85 hPa isobar, corresponding to downward motion [*Sherwood*, 2000]. *Fueglistaler et al.* [2004] extended the analysis of *Sherwood* [2000], *Simmons et al.* [1999] and *Hatsushika and Yamazaki* [2003] of the vertical ω wind fields at the 85 hPa and 90 hPa pressure surfaces and considered changes in potential temperature along kinematic trajectories. The trajectory study of *Fueglistaler et al.* [2004], with ω taken from ECMWF analysis, also showed subsidence (across isentropes) above the maritime continent.

[51] Following the line of argument of *Fueglistaler et al.* [2004], we find the existence of a region of subsidence in the upper TTL to be extremely sensitive to the chosen diabatic or kinematic scenario. Figure 6 shows that diabatic heating processes yield a mean vertical velocity field, which varies in the zonal and meridional directions, but remains nonnegative throughout the range of the TTL. The local minimum in the total diabatic upward velocity above the maritime continent (black rectangle in Figure 6) appears as a region of negative (downward) cross-isentropic velocity in the kinematic scenarios, consistent with the findings of *Fueglistaler et al.* [2004]. Thus, while in a diabatic world, there is almost no subsidence in the upper TTL, in a kinematic world, subsidence occurs rather frequently. The assimilation increment scenario also shows this subsidence, albeit much less pronounced.

[52] The consideration of the spread around the mean $d\theta/dt$ values in each horizontal grid box of Figure 6 (not shown) reveals that for the ω-INT and the asi-INT scenarios the standard deviation is similar to the mean values. For csk-INT and tot-INT the standard deviation is much lower. Thus the interpretation of the regions of negative mean cross-isentropic velocity (in the kinematic scenarios) as regions of subsidence does not seem reliable after all.

[53] Discussing possible reasons for the discrepancies between the diabatic and the kinematic scenarios is beyond the scope of this work. Therefore we simply state that within the framework of ERA-Interim the variability in the pressure tendency wind field cannot be traced back to structures in diabatic heating.

[54] Furthermore, as a result of section 3, none of the scenarios seems to contradict the results of *Folkins et al.* [1999], who reported on air masses in the TTL originating from the lower stratosphere. There is only the open question of whether this air descended from the stratospheric overworld or was quasi-isentropically in-mixed from the extratropical lowermost stratosphere, which is answered differently when different vertical velocity schemes are employed.

5.1.2. Vertical Dispersion

[55] A consideration of vertical dispersion confirms the occurrence of subsidence in the kinematic scenarios. Figure 7 shows that only for the kinematic scenarios and for the asi-INT scenario there are trajectories localized above their initial θ level after 60 days of backward integration. In agreement with *Schoeberl et al.* [2003], we find that for the kinematic scenarios, there is a much higher vertical dispersion than for the diabatic scenarios. The dispersive characteristics of the assimilation increment scenario are in between.

[56] From the two bottom plots of Figure 7, a reduction in vertical dispersion (noise) for the interim compared to the operational ω winds is evident, consistent with the results of *Monge-Sanz et al.* [2007].

5.1.3. Time Scales

[57] The speed of upward transport to the stratospheric overworld is a major determinant for propagation of tape recorder signals (e.g., water vapor [*Mote et al.*, 1996]). Moreover, corresponding transport time scales and pathways are crucial for determining the amount of very short-lived substances (VSLS) and other trace gases in the stratosphere. *Levine et al.* [2007, 2008] emphasized that VSLS easily reach the extratropical regions of the stratosphere, being meridionally transported out of the tropics. Below, we point out that modeling of these processes will depend on the scheme of vertical velocities.

[58] The most striking difference when comparing the kinematic and diabatic approaches is the stronger tropical upwelling in the kinematic scenarios, resulting in shorter residence times (Figure 8 and Table 2) and larger fractions of backward trajectories ascending from lower potential temperatures (Figure 5). The fastest upwelling results for operational ω. Upwelling due to the interim ω is weaker and not much stronger than for the total diabatic heating rate scenario. Consistent with a weaker tropical upwelling there is a smaller fraction of air entering the TTL directly from below (from the tropical troposphere), but a larger fraction

Table 3. Sensitive Versus Robust Characteristics of Transport in the TTL With Respect to the Vertical Wind Scheme

	Characteristics
Sensitive	Subsidence in the TTL:
	stratospheric drain above the maritime continent
	Vertical dispersion
	Residence times in the TTL
	Pathways in the TTL:
	tropical easterlies versus subtropical westerlies;
	traveled horizontal distance
Robust	In-mixing:
	about 25/33–50% (trajectories from poleward ±35°
	equ. lat.) for boreal winter/summer
	Hemispheric asymmetry:
	enlarged in-mixing from summer hemisphere
	Gates to the TTL:
	vertical: above Western Pacific (boreal winter)/
	Western Pacific–South China Sea–Northern India
	(summer);
	meridional: above Western Pacific (winter)/
	Western Pacific–Northern India (summer)
	Residence time enhancement:
	between 350–380 K

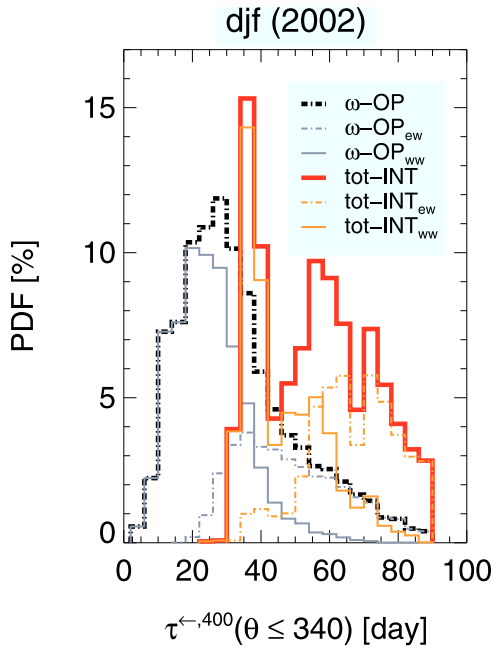

Figure 10. Formation of the two-peak shape of the transit time distribution of parcels at 400 K for ascending from 340 K. The thin gray and orange solid/dash-dotted lines denote the transit time distributions for net westward/eastward traveling trajectories. The bin size is 4 days.

which is meridionally in-mixed from the extratropics (Figure 4).

[59] The weaker ascent of air in the tropics in the diabatic scenarios is also reflected in the distribution of transit times from below the TTL to its upper part, in Figure 9. The time for ascent from 340 K to 400 K for total diabatic heating equals approximately 2 months (56/64 days for djf/jja) and is therefore about 10 days longer than for the interim and about 1 month longer than for the operational ECMWF kinematic scenario. These large differences in transit time scales are likely to influence the results of modeling the transport and chemistry of VSLS and other species.

[60] Moreover, Table 2 reveals that heating rates for asi-INT result in a faster circulation for boreal summer than for boreal winter. Thus the assimilation increment results in an inverted seasonality of upwelling, compared to the other scenarios.

[61] Concerning the formation of the head of the tape recorder, the time scale for ascending from the Lagrangian cold point (the minimum temperature along the trajectories) around 370 K to the stratospheric overworld is crucial. Table 2 shows that for ω from ERA-Interim or the total diabatic heating rate as vertical velocity, the respective time scale is more than twice as long as for operational ω. It remains to be shown in a future study whether these extended time scales are long enough to better represent tape recorder phenomena.

[62] However, we want to emphasize that differences in transport time scales due to the choice of vertical winds are large, even large enough to dwarf differences between seasons, regions and different years [*Krüger et al.*, 2009].

5.1.4. Pathways

[63] To further illustrate the evolution of the two-peak structure in the transit time distribution in Figure 9, we calculate the transit time distribution separately for trajectories traveling with the subtropical westerly jet and for the remaining trajectories, for the total diabatic heating scenario for boreal winter.

[64] Analogously to the analysis of *Fueglistaler et al.* [2004], trajectories with a maximum net zonal displacement during integration time of at least $\Delta\lambda = 180°$E are regarded as traveling with the strong westerly jets. Of course, this separation is not perfect, as it does not account for different pathways of trajectories with $\Delta\lambda < 180°$E, which can be eastward or westward traveling or confined to large anticyclonic systems (e.g., monsoons). However, even this simplified separation will provide a rather clear picture of which pathways contribute to which peak.

[65] Figure 10 shows that trajectories with $\Delta\lambda < 180°$E (tropical easterlies; thin solid orange line) mainly contribute to the fast and trajectories with $\Delta\lambda \geq 180°$E (subtropical westerlies; thin dash-dotted orange line) mainly to the second slower peak. A comparison of the horizontal distances traveled reveals large differences. On average, westward displaced total diabatic trajectories travel a horizontal distance of 44,000 km, while eastward displaced trajectories (about 46% of all trajectories) almost twice as far (83,000 km). For the operational kinematic scenario, westerly jet trajectories (35%) travel on average 65,000 km and the remaining trajectories about 24,000 km and hence much shorter distances.

[66] To summarize, we characterize the first (fast) pathway across the TTL as being tropically confined to the domains of fastest upwelling, with only small meridional and westward zonal displacements, mainly due to the tropical easterlies. Air which takes the second pathway rapidly ascends to ~350 K, where the ascent slows down because of a distinct minimum in upward velocity (enhanced residence times). Due to the slower ascent, the upwelling air is exposed to meridional drifts for a longer time and easily reaches the regions of the subtropical jets. The strong eastward horizontal flow of the jet stream displaces the air masses very far outside the regions of fastest upwelling, so that they ascend even slower and are displaced even farther. On their way to the stratospheric overworld they frequently enter the extratropics, in agreement with the results of *Levine et al.* [2007, 2008]. However, parts of these air masses again enter the tropics at higher potential temperature levels and significantly contribute to the composition of the upper TTL. Though this second pathway is less evident in the transit time distribution of the stronger kinematic upwelling, for the slower upwelling of the diabatic scenarios it gains in importance.

[67] To summarize, the partitioning of ascending air between different pathways in the TTL and consequentially the traveled horizontal distance turns out to be extremely sensitive to the vertical velocity scheme.

5.2. Robust Transport Characteristics

5.2.1. Residence Time Enhancement

[68] Figure 8 shows a large sensitivity of residence times in the TTL to the choice of vertical velocities, as discussed in section 5.1.3. But a closer look reveals an enhancement

of residence times in the layer between 350–380 K compared to layers above and below, which robustly emerges from all scenarios.

[69] Below about 350 K upwelling is mainly due to convection, above about 380 K due to the Brewer-Dobson circulation. In the coupling region in between, the ascent slows down in all scenarios, resulting in residence times more than twice as long as below 350 K and above 380 K.

5.2.2. Gates to the TTL

[70] The regions where air enters the TTL are very similar for the different trajectory scenarios and coincide with results from earlier studies [*Chen*, 1995; *Fueglistaler et al.*, 2004]. The main vertical entry regions (across the lower TTL boundary, here 350 K) are located above the Western Pacific for boreal winter and are displaced northwestward above the equatorial Western Pacific, the South China Sea and Northern India for boreal summer.

[71] The in-mixed trajectories enter the TTL essentially at longitudes where the flow due to the two quasi-stationary anticyclones above the Western Pacific for boreal winter and due to the Asian/American monsoons for boreal summer is directed toward the equator (compare e.g., Figure 5a of *Fueglistaler et al.* [2009a]).

5.2.3. In-mixing and Hemispheric Asymmetry

[72] In-mixing from poleward of the ±35° equivalent latitude band turns out to be an important pathway into the TTL (compare also *Konopka et al.* [2009]), irrespective of the vertical velocity scheme. For the four most realistic scenarios (tot-INT, asi-INT, ω-INT, ω-OP), robustly about 25/33–50% of trajectories in the TTL are in-mixed across the meridional boundaries for boreal winter/summer.

[73] Furthermore, the hemispheric asymmetry in in-mixing, with usually more than twice as much in-mixing from the summer than from the winter hemisphere, is not dependent on the choice of vertical velocities. The maximum discrepancy between the summer and winter hemisphere robustly arises for boreal summer. Irrespective of the scenario, the hemispheric asymmetry of in-mixing is likely due to the strong Asian monsoon anticyclone [*Dunkerton*, 1995; *Gettelman et al.*, 2004b; *Randel and Park*, 2006], as the main in-mixing (for boreal summer) occurs in regions of equatorward flow of the anticyclonic circulation (as explained in section 5.2.2), in agreement with *Chen* [1995].

[74] We term the trajectories meridionally entering the TTL from poleward ±35° equivalent latitude in-mixed, irrespective of how far they reach into the extratropics (Figure 3 provides this additional information). Hence, the ensemble of in-mixed trajectories consists of trajectories which reach deeply into the extratropical stratosphere as well as of trajectories, which are only transported through the subtropical jet core and might originate in the troposphere 3 months previously. Also the latter encounter regions of strong mixing in the subtropical jets [*Pan et al.*, 2006] and in the real atmosphere are very likely to transport extratropical stratospheric air into the TTL. However, even if the large in-mixed fractions of 25/33–50% do not represent air masses from deep extratropical lowermost stratosphere regions, they emphasize the great importance of the subtropical jets as pathways for transport to the tropical stratospheric overworld. For a quantitative estimation of the impact of extratropical in-mixed air on the composition of the TTL, CTM studies must be employed.

[75] Furthermore, it would be interesting to study the pattern of in-mixing by using a time-varying tropopause criterion, motivated by the work of *Haynes and Shuckburgh* [2000]. For our work, focusing on sensitivity of transport study results with respect to the vertical velocity scheme, we consider a constant equivalent latitude value to be adequate, as most studies employ a constant PV or equivalent latitude criterion to separate troposphere and stratosphere.

6. Summary and Conclusions

[76] We considered backward trajectories in the TTL, with pressure tendencies and various contributions from the diabatic heating budget as vertical velocities in kinematic and diabatic scenarios, to estimate the impact of the vertical velocity scheme on transport characteristics. Our study confirms that all contributions to the diabatic heating budget (effects due to radiation with clouds and due to latent heat release, mixing and diffusive heating) are necessary for modeling transport from the troposphere to above the level of zero clear-sky radiative heating. Thus, either clear-sky or all-sky radiative heating alone as diabatic heating rate misses very important processes.

[77] Transport characteristics which sensitively depend on the vertical velocity scheme are classified as sensitive, characteristics emerging as a robust picture from all scenarios as robust. A first sensitive characteristic is residence times in the TTL. Pressure tendency from operational ECMWF data yields the fastest tropical upwelling and the shortest mean transit times from 340 K to 400 K of about a month. For the pressure tendency and total diabatic heating from ERA-Interim these time scales are found to be 1 month longer and for all-sky heating and residual heating even longer.

[78] Furthermore, there are differences in the pathways to the stratospheric overworld among the different scenarios. In kinematic scenarios regions of mean downward cross-isentropic motion occur in the upper TTL, while in diabatic scenarios air rises uniformly throughout the entire range of the TTL. The addition of assimilation increments to the total diabatic heating rate yields a scenario with frequent regions of mean downward cross-isentropic motion, closer to the kinematic than to the diabatic scenarios. However, the large spread of velocities around the mean in the kinematic scenarios casts doubt upon the interpretation of mean downward motion regions as regions of subsidence.

[79] For scenarios of stronger upwelling (here, operational kinematic scenario) rising air is mainly tropically confined to the regions of fastest ascent. For the weaker upwelling of ERA-Interim, trajectories are more likely to reach the regions of the subtropical jets and thus travel large horizontal distances before again entering the tropics above the jet core. Consequently, also the horizontal traveled distance is crucially impacted by the choice of vertical velocities.

[80] A robust characteristic is the enhancement of residence times in the lower TTL, between about 350–380 K, irrespective of the scenario. Furthermore, for all scenarios a large fraction of trajectories in the TTL is meridionally in-mixed into the TTL across the meridional boundaries, indicating the crucial importance of the subtropical jets as pathways for TST and a potentially large impact of transport from the extratropical lowermost stratosphere on budgets of trace gases in the TTL. Also a pronounced

hemispheric asymmetry of meridional in-mixing, with enhanced in-mixing from the summer hemisphere (maximum for boreal summer), appears unaffected by the vertical wind scheme.

[81] We emphasize that results from trajectory studies concerning sensitive transport characteristics are to be handled with care, as they are largely sensitive to uncertainties arising from the method. On the other hand, results referring to robust characteristics are less influenced by the method. Overall, with respect to results of transport studies in the TTL, we find much greater reliability in robust patterns of transport than in exact numbers.

[82] An important step toward improving the reliability of trajectory and CTM studies, particularly with respect to sensitive transport characteristics, would be finding the ''true vertical velocity'' of the atmosphere. Therefore, comparisons against high-resolution tracer measurements, that are suited to resolve the differences between the various scenarios, are needed. As long as this problem is not solved, our work provides a guideline for estimating the sensitivity of results due to the choice of the vertical velocity scheme.

[83] **Acknowledgments.** We thank S. Fueglistaler, P. Bechtold, and L. L. Pan for helpful discussions, N. Thomas for programming support, and the ECMWF for providing reanalysis data.

References

Andrews, D. G., J. R. Holton, and C. B. Leovy (1987), *Middle Atmosphere Dynamics*, Academic Press, San Diego, Calif.

Bonazzola, M., and P. H. Haynes (2004), A trajectory-based study of the tropical tropopause region, *J. Geophys. Res.*, *109*, D20112, doi:10.1029/2003JD004356.

Chen, P. (1995), Isentropic cross-tropopause mass exchange in the extratropics, *J. Geophys. Res.*, *100*(D8), 16,661–16,673.

Danielsen, E. F. (1982), A dehydration mechanism for the stratosphere, *Geophys. Res. Lett.*, *9*, 605–608.

Dunkerton, T. J. (1995), Evidence of meridional motion in the summer lower stratosphere adjacent to monsoon regions, *J. Geophys. Res.*, *100*(D8), 16,675–16,688.

Folkins, I., M. Loewenstein, J. Podolske, S. J. Oltmans, and M. Proffitt (1999), A barrier to vertical mixing at 14 km in the tropics: Evidence from ozonesondes and aircraft measurements, *J. Geophys. Res.*, *104*(D18), 22,095–22,102.

Fueglistaler, S., and Q. Fu (2006), Impact of clouds on radiative heating rates in the tropical lower stratosphere, *J. Geophys. Res.*, *111*, D23202, doi:10.1029/2006JD007273.

Fueglistaler, S., H. Wernli, and T. Peter (2004), Tropical troposphere-to-stratosphere transport inferred from trajectory calculations, *J. Geophys. Res.*, *109*, D03108, doi:10.1029/2003JD004069.

Fueglistaler, S., S. Bonazzola, P. H. Haynes, and T. Peter (2005), Stratospheric water vapor predicted from the lagrangian temperature history of air entering the stratosphere in the tropics, *J. Geophys. Res.*, *110*, D08107, doi:10.1029/2004JD005516.

Fueglistaler, S., A. E. Dessler, T. J. Dunkerton, I. Folkins, Q. Fu, and P. W. Mote (2009a), Tropical tropopause layer, *Rev. Geophys.*, *47*, RG1004, doi:10.1029/2008RG000267.

Fueglistaler, S., B. Legras, A. Beljaars, J. J. Morcrette, A. Simmons, A. M. Tompkins, and S. Uppala (2009b), The diabatic heat budget of the upper troposphere and lower/mid stratosphere in ECMWF reanalysis, *Q. J. R. Meteorol. Soc.*, *135*, 21–37, doi:10.1002/qj.361.

Gettelman, A., W. J. Randel, and F. Wu (2002), Transport of water vapor in the tropical tropopause layer, *Geophys. Res. Lett.*, *29*(1), 1009, doi:10.1029/2001GL013818.

Gettelman, A., P. M. de F. Forster, M. Fujiwara, Q. Fu, H. Vömel, L. K. Gohar, C. Johanson, and M. Ammerman (2004a), Radiation balance of the tropical tropopause layer, *J. Geophys. Res.*, *109*, D07103, doi:10.1029/2003JD004190.

Gettelman, A., D. E. Kinnison, and T. J. Dunkerton (2004b), Impact of monsoon circulations on the upper troposphere and lower stratosphere, *J. Geophys. Res.*, *109*, D22101, doi:10.1029/2004JD004878.

Hall, T. M., and R. A. Plumb (1994), Age as a diagnostic of stratospheric transport, *J. Geophys. Res.*, *99*(D1), 1059–1070.

Hatsushika, H., and K. Yamazaki (2003), Stratospheric drain over Indonesia and dehydration within the tropical tropopause layer diagnosed by air parcel trajectories, *J. Geophys. Res.*, *108*(D19), 4610, doi:10.1029/2002JD002986.

Haynes, P., and E. Shuckburgh (2000), Effective diffusivity as a diagnostic of atmospheric transport: 2. Troposphere and lower stratosphere, *J. Geophys. Res.*, *105*(D18), 22,795–22,810.

Holton, J. R., and A. Gettelman (2001), Horizontal transport and the dehydration of the stratosphere, *Geophys. Res. Lett.*, *28*, 2799–2802.

Holton, J. R., P. Haynes, M. E. McIntyre, A. R. Douglass, R. B. Rood, and L. Pfister (1995), Stratosphere-troposphere exchange, *Rev. Geophys*, *33*(4), 403–439.

James, R., M. Bonazzola, B. Legras, K. Surbled, and S. Fueglistaler (2008), Water vapor transport and dehydration above convective outflow during Asian monsoon, *Geophys. Res. Lett.*, *35*, L20810, doi:10.1029/2008GL035441.

Konopka, P., et al. (2007), Contribution of mixing to upward transport across the tropical tropopause layer (TTL), *Atmos. Chem. Phys.*, *7*, 3285–3308.

Konopka, P., J.-U. Grooß, F. Plöger, and R. Müller (2009), Annual cycle of horizontal in-mixing into the lower tropical stratosphere, *J. Geophys. Res.*, *114*, D19111, doi:10.1029/2009JD011955.

Kremser, S., I. Wohltmann, M. Rex, U. Langematz, M. Dameris, and M. Kunze (2009), Water vapour transport in the tropical tropopause region in coupled Chemistry-Climate Models and ERA-40 reanalysis data, *Atmos. Chem. Phys.*, *9*, 2679–2694.

Krüger, K., S. Tegtmeier, and M. Rex (2008), Long-term climatology of air mass transport through the tropical tropopause layer (TTL) during NH winter, *Atmos. Chem. Phys.*, *8*, 813–823.

Krüger, K., S. Tegtmeier, and M. Rex (2009), Variability of residence time in the tropical tropopause layer during northern hemisphere winter, *Atmos. Chem. Phys.*, *9*, 12,597–12,614.

Levine, J. G., P. Braesicke, N. R. P. Harris, N. S. Savage, and J. A. Pyle (2007), Pathways and timescales for troposphere-to-stratosphere transport via the tropical tropopause layer and their relevance for very short-lived substances, *J. Geophys. Res.*, *112*, D04308, doi:10.1029/2005JD006940.

Levine, J. G., P. Braesicke, N. R. P. Harris, and J. A. Pyle (2008), Seasonal and inter-annual variations in troposphere-to-stratosphere transport from the tropical tropopause layer, *Atmos. Chem. Phys.*, *8*, 3689–3703.

Marcy, T. P., et al. (2007), Measurements of trace gases in the tropical tropopause layer, *Atmos. Environ.*, *41*(34), 7253–7261, doi:10.1016/j.atmosenv.2007.05.032.

McKenna, D. S., P. Konopka, J.-U. Grooß, G. Günther, R. Müller, R. Spang, D. Offermann, and Y. Orsolini (2002), A new Chemical Lagrangian Model of the Stratosphere (CLaMS): 1. Formulation of advection and mixing, *J. Geophys. Res.*, *107*(D16), 4309, doi:10.1029/2000JD000114.

Monge-Sanz, B. M., M. P. Chipperfield, A. J. Simmons, and S. M. Uppala (2007), Mean age of air and transport in a CTM: Comparison of different ECMWF analyses, *Geophys. Res. Lett.*, *34*, L04801, doi:10.1029/2006GL028515.

Mote, P. W., et al. (1996), An atmospheric tape recorder: The imprint of tropical tropopause temperatures on stratospheric water vapor, *J. Geophys. Res.*, *101*(D2), 3989–4006.

Pan, L. L., P. Konopka, and E. V. Browell (2006), Observations and model simulations of mixing near the extratropical tropopause, *J. Geophys. Res.*, *111*, D05106, doi:10.1029/2005JD006480.

Randel, W. J., and M. Park (2006), Deep convective influence on the Asian summer monsoon anticyclone and associated tracer variability observed with Atmospheric Infrared Sounder (AIRS), *J. Geophys. Res.*, *111*, D12314, doi:10.1029/2005JD006490.

Ricaud, P., et al. (2007), Impact of land convection on troposphere-stratosphere exchange in the tropics, *Atmos. Chem. Phys.*, *7*, 5639–5657.

Schoeberl, M. R., A. R. Douglass, Z. X. Zhu, and S. Pawson (2003), A comparison of the lower stratospheric age spectra derived from a general circulation model and two data assimilation systems, *J. Geophys. Res.*, *108*(D3), 4113, doi:10.1029/2002JD002652.

Sherwood, S. C. (2000), A stratospheric 'drain' over the maritime continent, *Geophys. Res. Lett.*, *27*, 677–680.

Simmons, A. J., A. Untch, C. Jakob, P. Kållberg, and P. Unden (1999), Stratospheric water vapour and tropical tropopause temperatures in ECMWF analyses and multiyear simulations, *Q. J. R. Meteorol. Soc.*, *125*, 353–386.

Simmons, A., S. Uppala, S. Dee, and S. Kobayashi (2006), ERA-Interim: New ECMWF reanalysis products from 1989 onwards, *ECMWF Newsl.*, *110*, 25–35.

Sparling, L. C., J. A. Kettleborough, P. H. Haynes, M. E. McIntyre, J. E. Rosenfield, M. R. Schoeberl, and P. A. Newman (1997), Diabatic cross-isentropic dispersion in the lower stratosphere, *J. Geophys. Res.*, *102*(D22), 25,817–25,829.

Tuck, A. F., et al. (1997), The Brewer-Dobson circulation in the light of high altitude in situ aircraft observation, *Q. J. R. Meteorol. Soc.*, *123*, 1–69.

Uppala, S. M., et al. (2005), The ERA-40 re-analysis, *Q. J. R. Meteorol. Soc.*, *131*, 2961–3012, doi:10.1256/qj.04.176.

Uppala, S., S. Dee, S. Kobayashi, P. Berrisford, and A. Simmons (2008), Toward a climate data assimilation system: status update of ERA-Interim, *ECMWF Newsl.*, *115*, 12–18.

Waugh, D. W., and T. M. Hall (2002), Age of stratospheric air: Theory, observations, and models, *Rev. Geophys.*, *40*(4), 1010, doi:10.1029/2000RG000101.

Wohltmann, I., and M. Rex (2008), Improvement of vertical and residual velocities in pressure or hybrid sigma-pressure coordinates in analysis data in the stratosphere, *Atmos. Chem. Phys.*, *8*, 265–272.

J.-U. Grooß, G. Günther, P. Konopka, R. Müller, and F. Ploeger, Institute of Stratospheric Chemistry, Forschungszentrum Jülich, Jülich, Germany. (j.-u.grooss@fz-juelich.de; g.guenther@fz-juelich.de; p.konopka@fz-juelich.de; ro.mueller@fz-juelich.de; f.ploeger@fz-juelich.de)